A Model for Positive Corona Inception from Charged Ellipsoidal Thundercloud Hydrometeors

S. A. Peeters[1], S. Mirpour[1], C. Köhn[2], S. Nijdam[1]

[1]Eindhoven University of Technology, Department of Applied Physics, The Netherlands
[2]DTU Space, National Space Institute, Technical University of Denmark, Denmark

Key Points:

- Corona onset through hydrometeors is modelled using the self-sustaining condition of electron avalanches.
- An optimal ellipsoidal aspect ratio of 0.1 for corona inception for representative conditions is found.
- Lightning inception via ellipsoidal hydrometeors is found to be achievable in thundercloud conditions.

Corresponding author: S. A. Peeters, `s.a.peeters@student.tue.nl`

Abstract

Lightning is observed to incept in thundercloud electric fields below the threshold value E_k for discharge initiation. To explain this, the local enhancement of the electric field by hydrometeors is considered. The conditions for the onset of positive corona discharges are studied in air for ellipsoidal geometries. A hydrometeor is simulated as an individual charged conductor in zero ambient field; there is only a field generated by the charge on the hydrometeor surface. By doing so, the feasibility of corona inception from ellipsoidal hydrometeors can be formulated based on the self-sustaining condition of electron avalanches. For representative hydrometeor volumes and typical thundercloud pressure, values between $1.2\,E_k$ and $37\,E_k$ were found for the onset electric field at the tip of the ellipsoid. From simulations the required ambient electric field for corona onset from an uncharged hydrometeor can then be derived. This results in values between $0.07\,E_k$ and $0.8\,E_k$ for semi-axes aspect ratios between 0.01 and 1. The charge required on the hydrometeor surface for corona onset is minimum for semi-axes aspect ratios between 0.04 and 0.07 depending on the considered hydrometeor volume. For the simulated hydrometeors, the values of this onset charge for typical pressures are between $1500\,\mathrm{pC}$ and $3200\,\mathrm{pC}$. Including a size-correction for comparison to in situ measurement shows agreement with measured precipitation charges. From the results it is concluded that corona onset from ellipsoidal hydrometeors of a realistic volume can be achieved in thundercloud conditions for certain aspect ratios.

1 Introduction

One of the greatest unanswered questions in lightning physics is how lightning is initiated in a thunderstorm (Mazur, 2016; Petersen et al., 2008; Dwyer & Uman, 2014). From in situ measurements it is found that lightning initiates in thundercloud electric fields which are considerably lower than the breakdown electric field required for the inception of electric discharges (Stolzenburg & Marshall, 2009; Marshall et al., 1995). One of the most popular and widely corroborated theories explaining how this is possible is the hydrometeor theory (Mazur, 2016; Petersen et al., 2008). This theory states that hydrometeors - ice and water particles in thunderclouds - locally enhance the electric field, such that the breakdown field is exceeded, and lightning inception is enabled. In recent observations of narrow bipolar events in thunderstorms, which generally coincide with lightning initiation, clear evidence supporting the involvement of hydrometeors was obtained (Rison et al., 2016). The role of hydrometeors in lighting inception has been investigated in laboratory experiments (Petersen et al., 2015; Coquillat et al., 1995; R. F. Griffiths & Latham, 1974) with a main focus on corona onset, which is the initial stage of the formation of a lightning leader.

A corona discharge is the result of electrical breakdown, which occurs at the voltage where the insulating gas surrounding the electrode becomes electrically conductive. An electrical discharge is thus only possible when a critical voltage, the onset voltage V_0, on the electrode is reached. Equivalently, the electric field E in the discharge region should exceed the breakdown threshold field E_k and thus the field on the surface of the electrode should exceed the onset field E_0. The breakdown field scales linearly with pressure, and at a typical thundercloud altitude pressure of $0.4\,\mathrm{atm}$ this field has a value of about $10\,\mathrm{kV/cm}$ (Raizer, 1991a). The main mechanism of electrical breakdown is the electron avalanche. For electric fields above E_k, electrons can multiply by means of impact ionization of air molecules, thereby forming avalanches. In order to have a self-sustaining discharge, a constant source of seed electrons is required, which can be supplied by photoionization (Raizer, 1991b). The first group of electrons that collides with the gas molecules and leads to photoionization is known as the primary electron avalanche, and the subsequently formed second group of electrons that can give further photoionization is known as the secondary electron avalanche (see Figure 1). In air, the gas molecules that are dominant in emitting photons after collisions with free electrons are nitrogen molecules, and the gas molecules that are predominantly photoionized by these photons are oxygen molecules.

It should be noted that avalanche formation is a stochastic process, such that electron multiplication can also take place in fields (slightly) below the breakdown field. These contributions are briefly investigated but otherwise neglected in this work.

The onset of a corona discharge is typically defined by the discharge becoming self-sustaining. The self-sustaining criterion that is often applied is the amount of photons produced by the secondary avalanche being at least equal to those produced by the primary avalanche (Liu et al., 2012; Naidis, 2005). This condition is also adapted by the current work, which closely follows the structure of the work by Liu et al. (2012).

Depending on electrode polarity, corona discharges can be positive or negative. A popular hypothesis for lightning initiation is that the development of a positive streamer system, developed from a seed positive streamer from the corona on a hydrometeor, precedes and leads to negative breakdown (L. P. Babich et al., 2016; Petersen et al., 2008; C. T. Phelps & Griffiths, 1976; C. Phelps, 1974; Loeb, 1966). Therefore, positive corona discharges are of great interest when investigating the initial stage of lightning initiation.

Laboratory experiments have revealed that the onset of a corona discharge strongly depends on the size and shape of the hydrometeor. In their study on corona initiation from small ice crystals, Petersen et al. (2015) reported that the onset field E_0 decreases with hydrometeor length and that ice crystals with sharper tips promote glow coronae while inhibiting positive streamer formation. Moreover, they noted that the onset field increases linearly with the relative gas density $\delta = N/N_0$ (where N and N_0 are the actual and standard gas densities), meaning $E_0 \sim p/T$, with p the pressure and T the temperature. The decrease of the onset field with size is also found in many point-to-plane and rod-to-plane experiments using metal electrodes (D'Alessandro & Berger, 1999; Waters & Stark, 1975; Nasser & Heiszler, 1974; Schumann, 1923; Kip, 1938), which are observed to give corona onset voltages very similar to ice electrodes (Bandel, 1951).

In simulations, similar conclusions were reached. Dubinova et al. (2015) investigated discharge inception conditions for dielectric ellipsoidal hydrometeors and concluded that an increase in hydrometeor length yields stronger field enhancement, as does a decrease in hydrometeor tip radius. Hence, a longer, sharper hydrometeor generally requires a lower background electric field for the initiation of a discharge. Likewise, in simulations of streamer initiation from charged water drops L. P. Babich et al. (2016) found a lower threshold ambient field for larger drop sizes. Dubinova et al. (2015) also observed an optimal semi-axes aspect ratio for inception; though longer hydrometeors produce a higher electric field, the probability of discharge initiation decreases when they become too sharp, because the field enhancement becomes too localized at the tip. As this ratio fixes the ellipsoidal hydrometeor's shape, an optimal shape can be determined. Simulations (Riousset et al., 2020) also show the experimentally observed linear pressure dependence of discharge initiation. This is expected, as it follows from the pressure dependence of the breakdown field.

In addition to size, shape and air density, the onset of a corona discharge has been found to depend on the orientation, surface features and initial charge of the hydrometeor. R. F. Griffiths and Latham (1974) concluded from experimental studies on ice particles that onset fields in thundercloud regions are probably in the range of 400-500 kV/cm, which was later corrected by R. Griffiths (1975) to 350-450 kV/cm when taking into account the effect of charge on ice particles. Furthermore, R. F. Griffiths and Latham (1974) suggested that continuous corona discharges could be generated from thundercloud ice crystals at temperatures above -18 °C only. Of course, the gas density increases with decreasing temperature, explaining the subsequent increase of the onset field. Moreover, the surface conductivity decreases with decreasing temperature such that corona onset becomes less likely (R. F. Griffiths & Latham, 1974; Petersen et al., 2006), and generally smaller ice crystals are formed at lower temperatures (Petersen et al., 2006). In 2006, Petersen et al. (2006) demonstrated that corona discharges can initiate in temperatures down to -38 °C, showing that corona and streamer discharges can initiate from hydrometeors at thundercloud altitudes relevant for lightning initiation. Moreover, from numerical simulations L. Babich et al. (2017) observed that the required charge on hydrom-

eteors at these representative temperatures and altitudes agrees with measured thundercloud precipitation charges, which are generally between 10 and 200 pC and for a small fraction of hydrometeors between 200 and 400 pC (Marshall & Winn, 1982).

To conclude, these studies reveal that the onset of a corona discharge from a hydrometeor depends on its size, shape and surface charge, and on environmental conditions such as pressure, temperature and the ambient electric field. Experimental results and in situ measurements indicate the essential role of hydrometeors in lightning initiation. These findings are supported by simulations of lightning inception from ice and water particles.

The comparison of experimental work on corona onset from ice point electrodes to measurements on metal point electrodes has shown the corona onset voltage to be very comparable (Bandel, 1951). To simulate the onset of a positive corona discharge from a metal electrode in air, Naidis (2005) introduced a model giving a corona inception criterion taking into account the ambient pressure and the size and shape of the electrode. This model was applied to spherical and cylindrical electrodes, and later revisited by Liu et al. (2012) for the spherical case.

The main goal of this paper is to extend this model to include another representative shape, the prolate spheroid, as ice and water particles in a thundercloud can have a wide variety of shapes depending on thundercloud conditions. Their sizes range from a few micrometers to several centimeters (MacGorman et al., 1998). The size distribution of hydrometeors is little investigated within thunderclouds due to difficulties of in situ measurements (Mazur, 2016), but it is expected that the extreme cases of several centimeters are rare, and that a millimeter range is more representative (Weinheimer et al., 1991; Gardiner et al., 1985). When these hydrometeors fall downwards due to gravity, they are extended along the vertical direction. The shape of the hydrometeor in the direction perpendicular to the thundercloud electric field has a negligible contribution to the field enhancement. More precisely, the enhancement at the tips is mainly determined by the length of the hydrometeor and the radius of curvature of the tip of the hydrometeor (Köhn & Ebert, 2015; Dubinova et al., 2015). Taking this into account, it can prove fruitful to investigate ellipsoidal hydrometeors. More specifically, assuming cylindrically symmetric thundercloud conditions, a prolate ellipsoid of revolution, or prolate spheroid, is considered.

Thus, the purpose of this study is to simulate positive corona discharges originating from a positively charged spheroidal hydrometeor tip. In doing so, the feasibility of lightning initiation from a spheroidal hydrometeor is studied. The simulation of this configuration is done using the model for the onset of positive corona discharges introduced by Naidis (2005) and further elaborated by Liu et al. (2012). The investigated hydrometeor is isolated and without ambient electric field. Thus, there is only an electric field generated by the charge on the hydrometeor, which differs from realistic lightning occurrences, where there is also an external field present due to the large-scale charge distribution. However, the effects of the field induced by a charged particle can already reveal a lot about the role of particle shape and size in discharge inception. Hence, for the charged hydrometeor the dependence of corona onset on its semi-axes aspect ratio and volume is reported for various ambient pressures by varying its major and minor axes.

2 Model Description

As elaborated, a corona discharge is the result of electrical breakdown via direct impact ionization within avalanches. The resulting avalanches are seeded by electrons supplied through photoionization. Taking loss by attachment processes into account, $\alpha = \eta$ defines electrical breakdown, where α is the number of ionizing collisions per unit length and η the number of electron attachments per unit length. Formulating the net ionization coefficient $\alpha_{eff} = \alpha - \eta$, breakdown is defined by $\alpha_{eff} = 0$. Of course these coefficients depend on the electric field E, meaning $\alpha_{eff} = 0$ determines the breakdown field E_k.

The number of photons produced by a primary avalanche is denoted by N_1, and those produced by a secondary avalanche by N_2. N_2 depends on N_1 through $N_2 = \gamma N_1$, where γ is the mean number of photons from the secondary avalanche produced by one of the photons from the primary avalanche (see Figure 1). In short, γ is the multiplication factor. Naidis (2005) formulates the criterion for corona inception as the secondary avalanche producing at least as many photons as the primary avalanche, so $N_2 = N_1$, or equivalently $\gamma = 1$. Then, the discharge is self-sustaining; it can proceed without external ionization sources. This criterion does not take into account the stochastic nature of discharge inception. The region around the hydrometeor where the breakdown field is exceeded is sufficiently small such that individual electron avalanches, which have an intrinsically random nature, should be considered. Here, the randomness, and therefore contributions from outside this region, is neglected, as only the total amount of electrons in the avalanche is investigated. The inclusion of stochastic effects would soften the criterion, as then electrons can 'tunnel' to higher energies (Rutjes, 2018).

For point and wire electrodes, most of the electrons and photons are produced near the surface of the electrodes. It is therefore a reasonable assumption that all photons that lead to photoionization are produced at the electrode surface. This assumption overestimates the effect of photoionization, as the effect of photons on electron production is now maximized. As will be further substantiated, this paper studies the minimum conditions for the onset of a corona discharge, such that this assumption is acceptable. Besides inducing photoionization and thereby triggering secondary electron avalanches, a photon can also fall back to the electrode surface or leave the ionization region and consequently not contribute to the secondary avalanche. Different factors, such as the photon absorption probability, affect this balance and thus play a role in satisfying the $\gamma = 1$ criterion for positive corona onset.
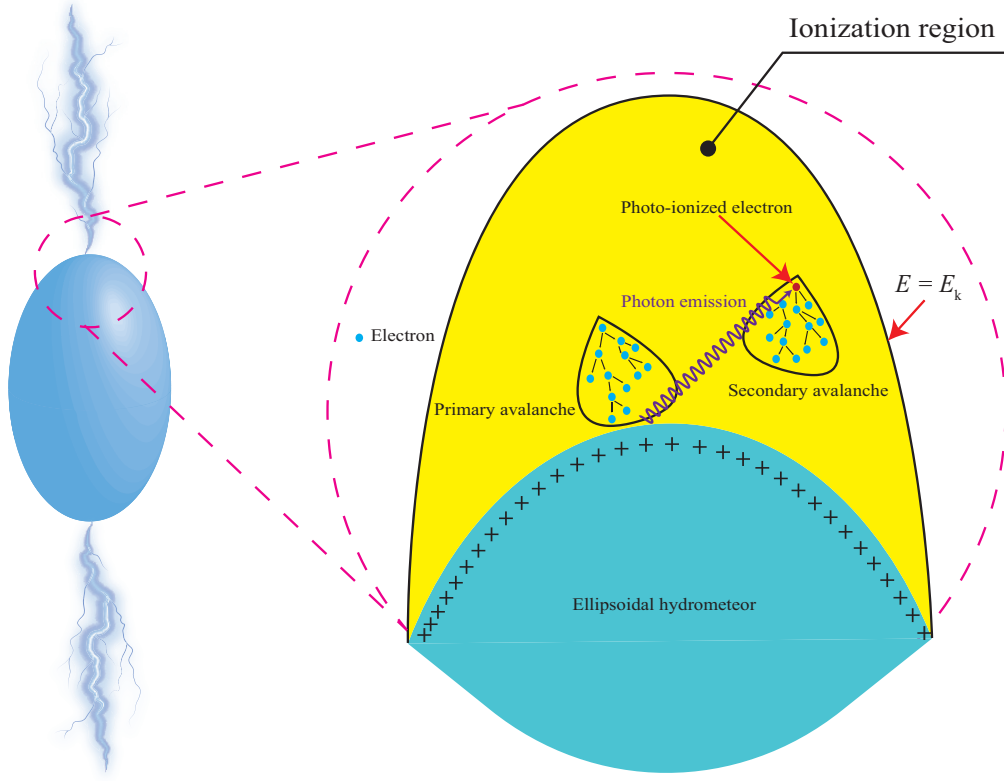
To formulate the $\gamma = 1$ criterion, a spherical coordinate system (r, θ, ϕ) is introduced with its origin at the surface of the electrode. This is illustrated in Figure 2 for the ellipsoidal electrode, with major axis a and minor axis b, considered in this paper. In the region near the electrode tip the electric field E reaches its maximum. Consequently, the number of electrons in the primary avalanche and the probability of photon emission are also maximum near the tip. For simplicity, it is assumed that the primary photon is emitted at the origin of the spherical coordinate system. Taking into account all possible directions in which this photon can move, the photon absorption region can be defined as the part of the ionization region ($E \geq E_k$) where $\theta \leq \pi/2$. In other words, the photon absorption region is the region that can be reached by the photon and where the field is sufficiently high such that an electron avalanche can be created. This region, highlighted in deep yellow in Figure 2, is thus the region of interest for the initiation of a corona discharge.

The corona inception criterion $\gamma = 1$, derived by Naidis (2005) using the above self-sustaining criterion, is then formulated as

$$\gamma \approx \xi \beta(\rho_0) \int_0^{2\pi} d\phi \int_0^{\pi/2} \sin\theta d\theta \int_0^{r_{max}(E)} r^2 P(r) \cdot \left[\exp\left(\int_{\rho_0(\theta,\phi)}^{\rho_{ab}(r,\theta,\phi)} \alpha_{eff}(\rho, E) d\rho \right) - 1 \right] dr = 1. \tag{1}$$

The coordinates ρ, r and θ are defined in Figure 2. Because of the cylindrical symmetry of the prolate spheroid, there is no ϕ-dependence. Besides the spherical coordinate system (r, θ, ϕ) with the origin at the tip of the ellipsoid, the coordinate ρ, which is given by the direction of the electric field and starts from the z-axis, is introduced as well, as is the radial coordinate ρ' from the center of the ellipsoid.

The term ξ is the ionization probability of an oxygen molecule at photon absorption. The distance $\rho_{ab}(r, \theta, \phi)$ is the distance between the point of photoionization (equivalent to the position of photon absorption) and the symmetry axis of the ellipsoid along the direction of the electric field in the point of photoionization. It is thus the length of

Figure 1. An illustrative image (not to scale) of the inception process in which the primary avalanche releases energetic photons, leading to the production of a photo-ionized electron. The secondary avalanche is formed by the multiplication of the photo-ionized electron via direct impact ionization. Inception occurs when the number of electrons in the secondary avalanche and the primary avalanche are equal. All processes occur in the photon absorption area, where the electric field is higher than the breakdown field (E_k).
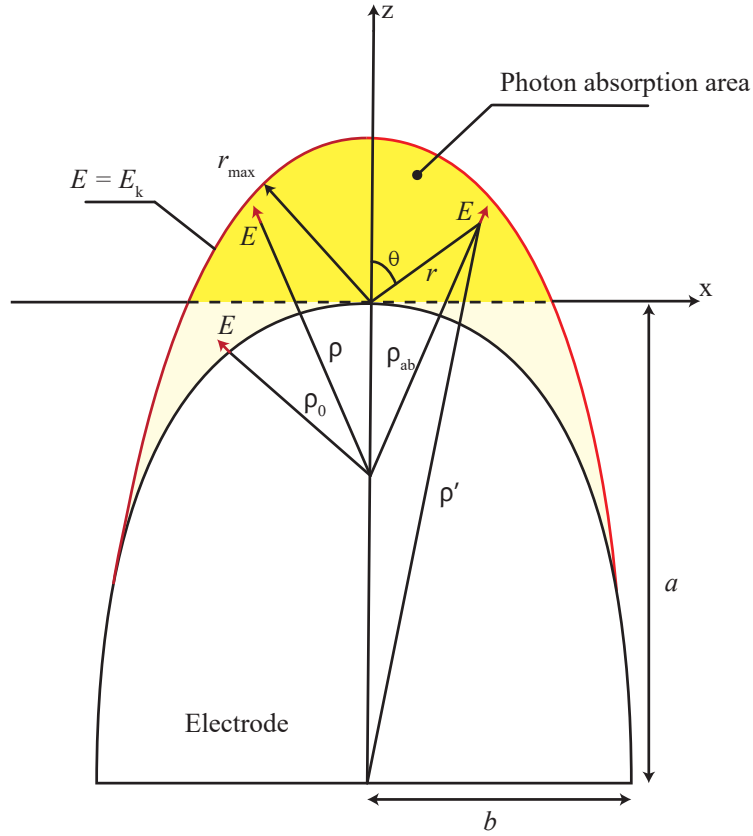
223   the line along the ρ coordinate that ends at the point of photon absorption (see Figure
224   2). Similarly, the distance from the symmetry axis of the ellipsoid to its surface along
225   the surface electric field direction is given by ρ_0 (for a sphere this would be its radius).
226   The position where the electric field has decreased to the breakdown field E_k is given
227   by r_{max} in the spherical coordinate system (r, θ, ϕ). Naidis (2005) uses the expression for
228   the photon absorption probability $P(r)$ in air where photoionization of oxygen molecules
229   takes place at absorption of radiation of wavelengths 98 - 102.5 nm, emitted by nitro-
230   gen molecules (Zhelezniak et al., 1982)

$$P(r) = \frac{\exp\left(-\kappa_1 r \delta\right) - \exp\left(-\kappa_2 r \delta\right)}{4 \pi r^3 \log\left(\kappa_2 / \kappa_1\right)}, \tag{2}$$

231   where $\kappa_1 = 5.6\,\mathrm{cm}^{-1}$ and $\kappa_2 = 320\,\mathrm{cm}^{-1}$. The term $\xi \beta(\rho_0)$ can be found from

$$\xi\beta = \left(0.03 + \frac{3.78}{E}\right)\frac{\delta_q}{\delta + \delta_q},\tag{3}$$

where $\delta_q = 0.04$ and E is the electric field (Zhelezniak et al., 1982). Here β is the
coefficient of production of ionizing photons scaled to the net ionization coefficient α_{eff}.
Because of its weak dependence on the electric field and the high fields at the electrode
surface, β is approximated by its value $\beta(\rho_0)$ at the surface. To apply the corona incep-
tion criterion $\gamma = 1$ to a prolate spheroid, analytical expressions should be derived for
the distances r_{max}, ρ_0 and ρ_{ab}, and the electric field E, on which the ionization prob-
ability and the net ionization coefficient depend.

Figure 2. A schematic of the photon absorption area around a positive ellipsoidal electrode.

To determine ρ_{ab}, the direction of the electric field is needed. This direction is given
by the bisector of the two straight lines from the focal points of the prolate spheroid to
the observation point (Curtright et al., 2020). Using various trigonometric relations, which
are given in the supporting information, it can be derived that

$$\rho_{ab} = \frac{\sqrt{2}\rho_1{}^2\sqrt{\frac{\left(4\sqrt{a^2-b^2}(a+r\cos(\theta))+\rho_1{}^2\right)\left(2ar\cos(\theta)+b^2+\rho_1\rho_2+r^2\right)}{\rho_1\rho_2}}}{\rho_1{}^2 + \rho_1\rho_2},\tag{4}$$

with ρ_1 and ρ_2 the straight lines from the two focal points of the ellipsoid to the
observation point (see also the supporting information) given by

$$\rho_{1,2} = \sqrt{r^2 + (a \mp \sqrt{a^2 - b^2})^2 + 2(a \mp \sqrt{a^2 - b^2})r\cos\theta} \tag{5}$$

Using the derived expression for ρ_{ab}, the distance ρ_0 can be formulated. This is done by formulating the equation of the ellipsoid with the origin at its tip, using the coordinate system (r, θ, ϕ). By solving the ellipsoid equation ($\frac{x^2}{b^2} + \frac{y^2}{b^2} + \frac{z^2}{a^2} = 1$ rewritten in the considered coordinates) for r and substituting r in the expression for ρ_{ab}, ρ_{ab} is constrained to the surface of the ellipse and thus ρ_0 is obtained. Because the surface of an ellipsoid and $\mathbb{R}^3$ do not form a diffeomorphic pair, two expressions for r are obtained and therefore two expressions for ρ_0. These expressions are valid separately for $\theta \le \pi/2$ and $\theta > \pi/2$ and are given in Appendix A.

The electric field of a conducting ellipsoid has been derived analytically by Köhn and Ebert (2015) for the prolate spheroid case and by Curtright et al. (2020) for arbitrary dimensions. The derivation of the electric field strength E yields

$$E(x, y, z) = \frac{Q}{4\pi\epsilon_0} \left(\prod_{k=1}^{3} \frac{1}{\sqrt{a_k^2 + \Theta(\vec{r})}} \right) \Big/ \sqrt{\left(\sum_{m=1}^{3} \frac{x_m^2}{(a_m^2 + \Theta(\vec{r}))^2} \right)}, \tag{6}$$

where Q is the total charge on the ellipsoid surface, ϵ_0 is the vacuum permittivity, $\Theta(\vec{r})$ the equipotential surfaces and $a_1 = a_x = b$, $a_2 = a_y = b$ and $a_3 = a_z = a$ are the semi-axes of the considered spheroid of Figure 2. Moreover, the Θ-equipotentials follow from

$$\sum_{k=1}^{3} \frac{x_k^2}{a_k^2 + \Theta(\vec{r})} = 1, \text{ for } \Theta(\vec{r}) > 0. \tag{7}$$

The above electric field expression can be rewritten in the considered coordinates (ρ', r, θ, ϕ) as defined in Figure 2. Here r can be converted to ρ' using the trigonometric relation $\rho' = \sqrt{a^2 + r^2 + 2ar\cos(\theta)}$. The field is also reformulated to contain the electric field at the ellipsoid tip ($z = a$ in equation (6)) $E_0 = \frac{Q}{4\pi b^2 \epsilon_0}$. To obtain the final expression for the electric field, the ρ' coordinate is converted to the ρ coordinate along the electric field direction as required for the $\gamma = 1$ criterion. This is done using the derived ρ_{ab} expression. In order to have analytically solvable equations in this derivation, r is not converted to ρ' in the conversion from ρ' to ρ. This means some ambiguity remains in the expression of the electric field $E = E(\rho, r, \theta)$. As eventually the equation $\gamma = 1$ is solved numerically, this ambiguity is not a problem as long as the resulting α_{eff} (which is calculated using the electric field) behaves correctly. The used formulation is

$$E(\rho, r, \theta) = \frac{2b^2 E_0 \rho'}{\sqrt{a^2 - b^2 + q + \rho'^2} \left(-a^2 + b^2 + q + \rho'^2 \right) \sqrt{\frac{q}{\frac{(b^2 - a^2)(a^2 + 2ar\cos(\theta) + r^2\cos(2\theta))}{a^2 + 2ar\cos(\theta) + r^2} + q + \rho'^2}}}, \tag{8}$$

with the shorthand $q = \sqrt{\frac{2\rho'^2(b^2 - a^2)(a^2 + 2ar\cos(\theta) + r^2\cos(2\theta))}{a^2 + 2ar\cos(\theta) + r^2} + (a^2 - b^2)^2 + \rho'^4}$ and with

$$\rho' = \sqrt{\frac{2ar\cos(\theta)\left(3a^2 - 3b^2 + \rho^2\right) + 2a^2\rho^2 + a^2\rho_1\rho_2 - b^2\rho^2 - b^2\rho_1\rho_2 + \rho^2 r^2 + \rho^2\rho_1\rho_2 + p}{2a^2 + 2ar\cos(\theta) - b^2 + r^2 + \rho_1\rho_2}}, \tag{9}$$

with $p = 2a^4 - a^2b^2 + 2a^2r^2\cos(2\theta) + a^2r^2 - b^4 - 2b^2r^2\cos(2\theta) - b^2r^2$. The derivations of these expressions are presented in the supporting information.

Finally, the distance r_{max} from the tip of the prolate spheroid to the position where $E = E_k$ can be determined. Because there is no explicit solution for r_{max} in the considered geometry, this is done by approximating the surface $E = E_k$ as forming an ellipsoid surface near the tip, as is validated in simulations in the supporting information. Then, finding r_{max} specifically for $\theta = 0$ and $\theta = \pi/2$ is sufficient to obtain r_{max} for arbitrary θ. These expressions are found by reformulating the electric field in terms of r and θ only and solving $E(r, \theta = 0) = E_k$ and $E(r, \theta = \pi/2) = E_k$, the latter leading to a case known as 'Casus irreducibilis' (Wantzel, 1843). This yields an analytical expression for r_{max} which can be validated using the aforementioned simulations:

$$r_{max}(\theta) = \frac{r_{max}(\theta=\pi/2)\left(\sqrt{r_{max}(\theta=0)^2(2a+r_{max}(\theta=0))^2\sin^2(\theta)+r_{max}(\theta=\pi/2)^2(a+r_{max}(\theta=0))^2\cos^2(\theta)} - a r_{max}(\theta=\pi/2)\cos(\theta)\right)}{r_{max}(\theta=0)(2a+r_{max}(\theta=0))\sin^2(\theta)+r_{max}(\theta=\pi/2)^2\cos^2(\theta)}, \tag{10}$$

with the expressions for $r_{max}(\theta = 0)$ and $r_{max}(\theta = \pi/2)$ derived and given in the supporting information.

Using the now known required expressions, the surface electric field E_0 at the tip of the ellipsoidal hydrometeor required for the onset of a positive corona discharge can be calculated from equation (1) at the known electric field distribution $E(\rho, r, \theta)$ for different values of the relative gas density δ and major and minor axes a and b. As noted by Liu et al. (2012), it is more convenient to, instead of using $\gamma = 1$, define a new quantity:

$$Y \equiv \gamma - 1 = 0. \tag{11}$$

The onset surface electric field E_0 at the tip can now be computed by finding the zero of Y. This cannot be done analytically due to the complexity of the integrals. Moreover, since the integration limits in equation (1) also depend on the unknown E_0 and the integration variables, numerical integration by itself is also not sufficient. However, this numerical integration can be combined with a numerical function that finds the root of an expression, such as the MATLAB function 'fzero', as used by Liu et al. (2012) and this work, or the Mathematica function 'FindRoot'. Substituting the numerical integration of equation (11) into the find root function means the numerical integration can be solved even though the integration limits are not numbers. Thus, in combination with this method the model determines the corona onset field E_0 at the hydrometeor tip through equation (11), equivalent to equation (1).

After applying the find root function, the found onset field E_0 can be used to evaluate the ionization integral K, given by

$$K = \int_{\rho_0}^{\rho_c} \alpha_{eff}(\rho, E)d\rho, \tag{12}$$

where $\rho_c = \rho_{ab}(r_{max}, \theta, \phi)$ gives the position of the breakdown field E_k. Exponentiation of K yields the number of electrons produced by an avalanche from the edge of the ionization region to the surface of the hydrometeor. Equation (12) is thus a criterion for the onset of a positive corona discharge with K a threshold value that needs to be reached to enable initiation. It is important to note that the above integration is taken along the field line from the surface of the electrode to the edge of the ionization region, because the avalanche follows the direction of the electric field.

Per the convention used by Naidis (2005), the model is set up to output the onset field E_0, from which the onset voltage V_0, onset charge Q, and ionization integral K can be derived. This order is thus kept in the following results section.

As stated, the used model gives the minimum condition for the onset of a corona discharge. Besides assuming all photons are emitted at the surface, it neglects the presence of space charge created in the discharge. Furthermore, the onset criterion is only imposed on the secondary avalanche; further avalanches are assumed to take place when this criterion is satisfied. While these factors generally increase the threshold for corona inception, including its stochastic nature would lower this threshold. The validity of the model depends on the relevant dimensions. For the model to be reliable, the largest photon absorption length (r_{max}) should be smaller than the length of the ellipsoid. Otherwise, the equilibrium between the ionization coefficients with the local electric field cannot be guaranteed.
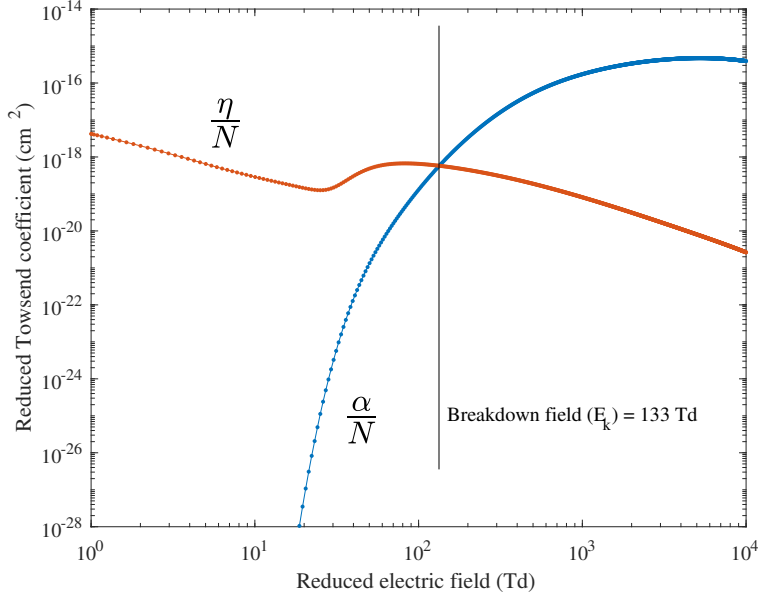
3 Results and discussions

3.1 The effects of varying aspect ratio and volume of spheroidal hydrometeors on the corona inception criterion

To calculate the required effective ionization coefficient α_{eff} in equation (1), we need to use the air plasma-chemical reactions which are listed in Table 1. All electron impact ionization, excitation, elastic and attachment reactions (except three-body attachment) that are included in the list were taken from Itikawa database (*Itikawa database, www.lxcat.net, retrieved on Sep 15, 2020.*, n.d.; Itikawa, 2005, 2008). The three-body attachment with O_2 as the third body was taken from Phelps database (*Phelps database, www.lxcat.net, retrieved on Sep 15, 2020.*, n.d.) and scaled to the different δ. Next, the reactions were used as input for BOLSIG+ (Hagelaar & Pitchford, 2005; *BOLSIG+ solver ver. Windows 12/2019*, n.d.) to calculate the ionization and attachment coefficients. The results are depicted in Figure 3 and the effective ionization coefficient is defined as the subtraction of the attachment coefficient from the ionization coefficient.

Table 1. List of plasma-chemical reactions used for calculation the ionization and attachment coefficients.

	Reaction
Elastic	$e^- + N_2 \rightarrow e^- + N_2$ $e^- + O_2 \rightarrow e^- + O_2$
Ionization	$e^- + N_2 \rightarrow 2e^- + N_2^+$ $e^- + N_2 \rightarrow 2e^- + N^+ + N$ $e^- + N_2 \rightarrow 3e^- + N^{2+} + N$ $e^- + O_2 \rightarrow 2e^- + O_2^+$ $e^- + O_2 \rightarrow 2e^- + O^+ + O$ $e^- + O_2 \rightarrow 3e^- + O^{2+} + O$
Attachment	$e^- + O_2 + O_2 \rightarrow O_2^- + O_2$ $e^- + O_2 \rightarrow O^- + O$
Excitation	$e^- + O_2 \rightarrow e^- + O_2^*$ $e^- + N_2 \rightarrow e^- + N_2^*$

Using the corona inception criterion of equation (1), equation (11) is solved numerically in MATLAB for varying hydrometeor volume $\frac{4}{3}\pi C$, with $C = ab^2$ the volume parameter, and varying aspect ratios b/a. The aspect ratio b/a is considered instead of, for
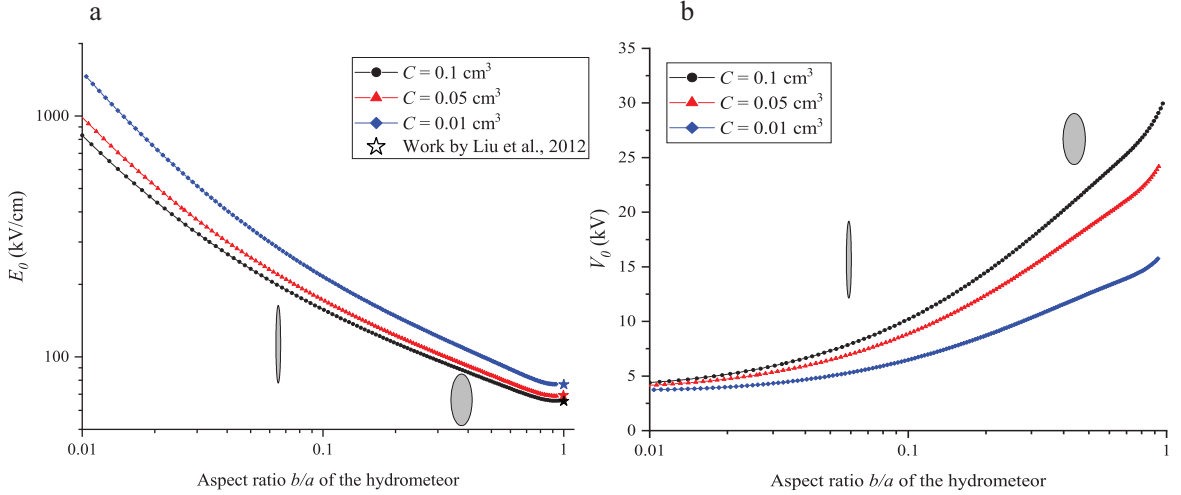
Figure 3. Reduced attachment (η/N) and ionization (α/N) coefficients as a function of reduced electric field in an $N_2 : O_2 = 80{:}20$ mixture at $\delta{=}1$. The breakdown field is determined where $\alpha - \eta{=}0$.

example, the major axis a, such that the effects of varying volume and shape can be investigated separately.

The studied hydrometeor geometries have volume parameters of $C = 0.01$, 0.05, and $0.1\,\mathrm{cm}^3$ and aspect ratios from $b/a = 0.01$ to 1, where $b/a = 1$ represents a sphere ($a = b$). First, positive corona inception is investigated at atmospheric pressure ($\delta = 1$). The onset field E_0 at the tip of the ellipsoid, found directly from solving equation (11), is presented in Figure 4a. It can be seen that E_0 decreases with volume for a fixed aspect ratio. For the smallest hydrometeor, $C = 0.01\,\mathrm{cm}^3$, the onset field at $b/a = 0.045$ is $366\,\mathrm{kV/cm}$, while for the largest hydrometeor, $C = 0.1\,\mathrm{cm}^3$, this is $248\,\mathrm{kV/cm}$. The decrease of the onset field with increasing volume is expected as a larger hydrometeor, simulated as an electrode, provides more surface for photon emission to the photon absorption region. Here, it should be noted that in the model it was assumed that all photons that lead to photoionization are emitted at the surface. Thus, for a smaller hydrometeor less photons are emitted and therefore less electrons are produced by photoionization, such that to satisfy the corona onset criterion a larger onset field E_0 is required.

From Figure 4a it can also be concluded that for a fixed volume, a sharper ellipsoid has a larger onset field E_0 at its tip. Because a sharper ellipsoid has less surface near the photon absorption region, a larger E_0 is needed to meet the inception criterion. In the spherical limit, $b/a = 1$, the onset field for $C = 0.01\,\mathrm{cm}^3$ is about 17% larger than that for $C = 0.1\,\mathrm{cm}^3$, and for the much sharper tip at $b/a \approx 0.015$ this difference has increased to about 70%. The onset field thus increases much stronger with sharpness for a smaller hydrometeor, which is expected as a smaller object has more surface area compared to its volume. It should be noted, however, that Figure 4a does not give the whole story. This onset field is only at the tip of the ellipsoid. Moreover, as charges on a conductor tend to move away from each other as much as possible on its surface, the electric field is enhanced more strongly near a sharper tip. Hence, even though a sharper ellipsoid has a larger E_0, this does not necessarily mean corona inception from sharper

hydrometeors in thunderstorms is less likely. On the contrary, Petersen et al. (2015) observed sharper hydrometeors promote glow coronae. R. F. Griffiths and Latham (1974) suggested in their paper on coronae from ice hydrometeors that the onset ambient field decreases with increasing combined length of the liquid filament, which was confirmed by Crabb and Latham (1974), who also found that the elongated filament resulting from raindrop collision promotes corona onset. This seems to contradict the decrease of E_0 with elongation in Figure 4a, but taking into account the mentioned effect of only considering the tip this discrepancy is explained. To draw clearer conclusions, other quantities such as potential, surface charge and the ionization integral should be considered as well when studying corona inception from an ellipsoid.
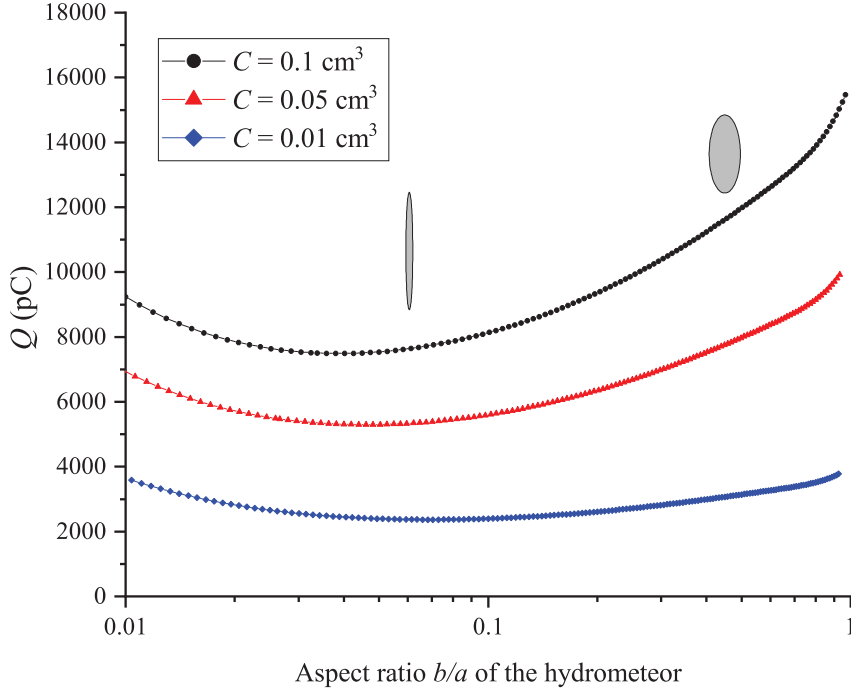

Figure 4. The a) onset field, and b) onset voltage for positive coronae at the tip of the ellipsoidal hydrometeor for $C = 0.01, 0.05,$ and $0.1\,\mathrm{cm}^3$ for varying aspect ratio b/a at atmospheric pressure. For clarity, two ellipsoid shapes are given at different b/a. Results are compared in the spherical limit ($b = a$) with Liu et al. (2012).

From the onset field E_0 the onset voltage, or inception voltage, along the major axis (from the tip to infinity) can be calculated by the integration of the electric field. This onset voltage V_0 is shown in Figure 4b. The inception voltage increases with hydrometeor volume. This is also found by Liu et al. (2012) for a spherical electrode. Note that the onset field decreases with volume while the onset voltage increases, which can be quickly understood by looking at the simpler configuration of a sphere, where $V_0 = E_0\rho_0$, with ρ_0 its radius. Figure 4b also shows that the onset voltage is lower for a sharper ellipsoid. For a very sharp tip this difference is less noticeable, and the onset voltage is about 4 kV for the three hydrometeors. In the spherical limit, the largest hydrometeor ($C = 0.1\,\mathrm{cm}^3$) requires 30 kV for corona onset, while the smallest hydrometeor ($C = 0.01\,\mathrm{cm}^3$) requires 16 kV.

Besides the onset voltage V_0, the onset charge Q can also be derived from the onset field E_0 through $E_0 = \frac{Q}{4\pi b^2 \epsilon_0}$. Of course, the onset field is a result of the onset charge, making this the more fundamental parameter. The onset charge, which is the total charge on the electrode surface, is depicted in Figure 5. A size-dependent optimum aspect ratio b/a is observed at which the onset charge is lowest. While a sharper ellipsoid has a higher onset field and thus requires more charge at the tip to reach this E_0, a larger fraction of the total charge is collected at its tip because of the optimization of charge separation. In simulations of corona inception from hydrometeors modelled as dielectrics in an external electric field, Dubinova et al. (2015) also found a size-dependent aspect

ratio for which the onset background field is minimum. From Figure 5 the range of onset charge for hydrometeors with volumes between $0.042\,\text{cm}^3$ and $0.42\,\text{cm}^3$ is found to be $2367\,\text{pC}$ to $15,467\,\text{pC}$ at atmospheric pressure.

Figure 5. The onset charge for positive coronae at the tip of the ellipsoidal hydrometeor for $C = 0.01$, 0.05, and $0.1\,\text{cm}^3$ for varying aspect ratio b/a at atmospheric pressure.

Finally, the ionization integral K along the major axis can be calculated from the onset field as well, through equation (12). The result is presented in Figure 6. At a fixed volume, the ionization integral decreases with b/a, meaning that less electrons are required in an avalanche from the edge of the photon absorption region to the electrode surface. To interpret these results the dependence of the photon absorption area and length on the electrode dimensions are studied in COMSOL for some data points, of which the results are given in Table 2. From this data it can be concluded that for a fixed aspect ratio, a smaller electrode has a smaller photon absorption area and length, as does a sharper electrode for a fixed volume. However, for a very sharp electrode the photon absorption area and length are approximately equal, as can be seen for $b/a = 0.014$ in Table 2.

As an ellipsoid with smaller b/a has a smaller photon absorption region, photons are absorbed closer to the electrode compared to its size, such that stronger avalanches are required to satisfy the inception criterion. A similar argument was made by Naidis (2005) to explain the ionization integral dependence on radius for a spherical and cylindrical electrode. Comparing the data points for different volumes, two regions can be discerned in Figure 6, separated by a cross-over point around $b/a = 0.55$. At large b/a, where K drops below 14, the largest ellipsoid has the largest value for the ionization integral, again because photons are absorbed closer to the electrode with respect to its size. When K increases above 14 for decreasing b/a it is observed that the smallest ellipsoid has the largest K value. An explanation for this could be that when b/a becomes small enough, the photon absorption region becomes so small that its absolute size instead of its relative size determines the value of the ionization integral. Stronger avalanches are then required for a smaller electrode. For very small b/a the data points for different vol-

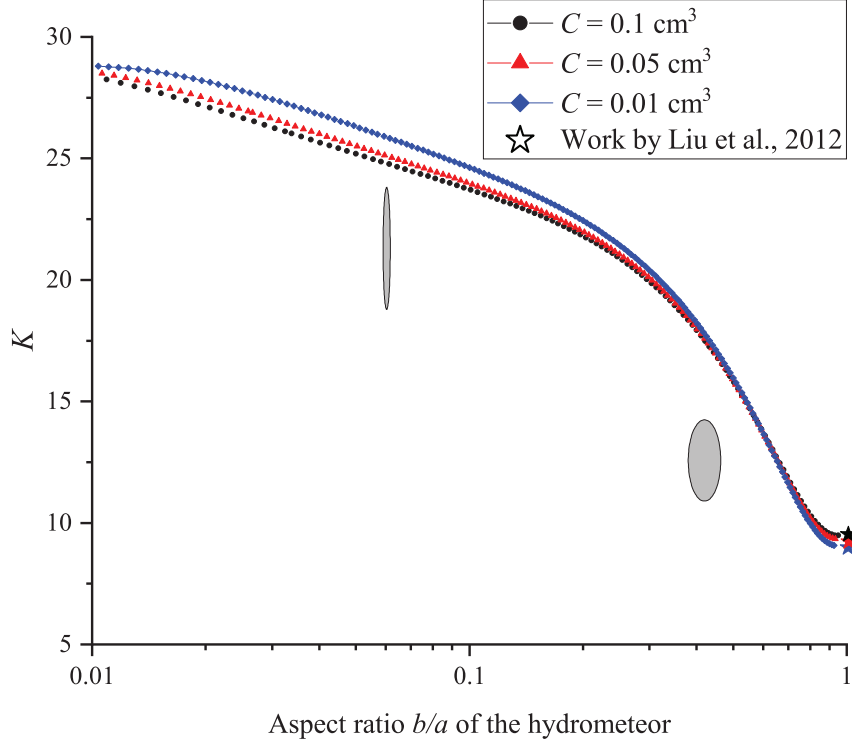**Table 2.** Photon absorption area and length for various ellipsoidal electrode aspect ratios and volumes.

Volume parameter C (cm^3)	Aspect ratio b/a	Semi axis a (cm)	Semi axis b (cm)	Area (mm^2)	Length r_{max} (mm)
0.1	0.014	7.93	0.11	0.21	0.12
0.1	0.045	3.68	0.16	0.33	0.22
0.1	0.141	1.70	0.24	1.02	0.47
0.1	0.447	0.79	0.35	6.20	1.02
0.05	0.014	6.29	0.08	0.25	0.11
0.05	0.045	2.92	0.13	0.28	0.20
0.05	0.141	1.35	0.19	0.84	0.41
0.05	0.447	0.62	0.28	4.91	0.88
0.01	0.014	3.68	0.05	0.25	0.09
0.01	0.045	1.70	0.07	0.28	0.16
0.01	0.141	0.79	0.11	0.58	0.31
0.01	0.447	0.36	0.16	2.71	0.61

umes appear to converge again. A likely explanation is that when the ellipsoid becomes very sharp, a photon is absorbed so close to the tip such that the total volume of the electrode has no effect; only the sharpness of the tip determines the value of the ionization integral. This is supported by the photon absorption area being approximately equal for the different volumes at $b/a = 0.014$ in Table 2.

3.2 Variation of the corona inception criterion with pressure

Next, the dependence of corona onset from an ellipsoidal hydrometeor on the ambient pressure is investigated by varying the relative gas density δ. More specifically, the values $\delta = 10$, 1, and 0.1, analogous to the works by Naidis (2005) and Liu et al. (2012), and $\delta = 0.5$, representative for thundercloud altitudes, are considered. The volume parameter is fixed at $C = 0.01\,\mathrm{cm}^3$ and the aspect ratio b/a varies again from $b/a = 0.01$ to 1. The results for the onset field at the hydrometeor tip are shown in Figure 7a. As expected, a higher pressure leads to a higher onset field E_0. As explained by Liu et al. (2012), at a higher pressure more of the excited nitrogen molecules responsible for emitting the ionizing photons are quenched, leading to a lower photon production such that a higher field is required. To briefly examine how the results are affected by the aforementioned photoionization outside of the ionization region, the computations are redone with an integration upper limit of $10r_{max}$ instead of r_{max}. It follows that the difference in outcome is generally well below 1%, only rising above 5% for $\delta = 0.5$ for the smallest volume parameter $C = 0.01\,\mathrm{cm}^3$, and only for very blunt tips, nearing $b/a \approx 1$. Neglecting this stochastic effect thus seems justified.

Similarly, the onset charge increases with pressure, as depicted in Figure 7b. For $C = 0.01\,\mathrm{cm}^3$ the onset charge is between $547\,\mathrm{pC}$ and $2400\,\mathrm{pC}$ for $\delta = 0.1$ and between $1500\,\mathrm{pC}$ and $3100\,\mathrm{pC}$ for $\delta = 0.5$. For $\delta = 0.5$ the onset charge is minimum at an aspect ratio of approximately 0.1. A pressure above atmospheric pressure, at $\delta = 10$, is not representative for thunderstorms, but is included for completeness. Again, the ionization integral K can be calculated from the onset field and is plotted in Figure 7c. The pressure dependence can be explained as before; due to increased quenching of excited nitrogen molecules at higher pressures the photon production is lowered. Therefore, stronger avalanches are required to satisfy the inception criterion.

Figure 6. The ionization integral along the major axis for positive corona onset at the tip of the ellipsoidal hydrometeor for $C = 0.01$, 0.05, and $0.1\,\text{cm}^3$ for varying aspect ratio b/a at atmospheric pressure.
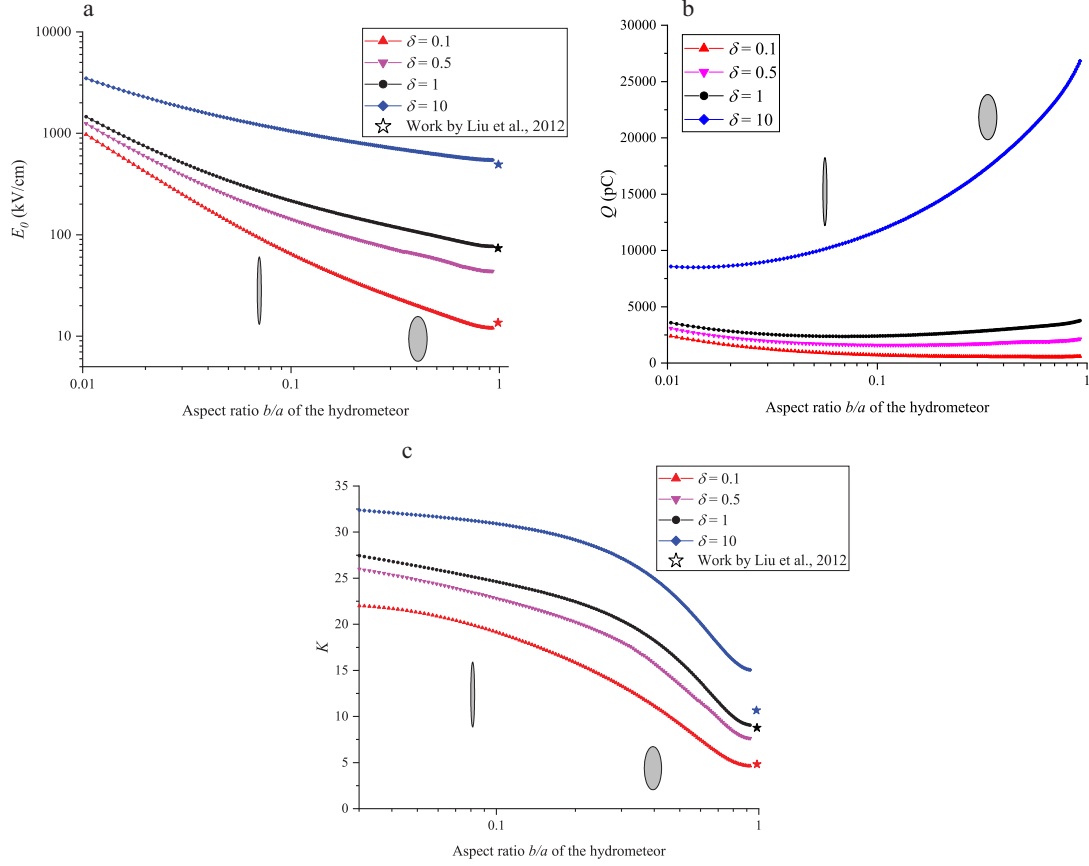
3.3 Dependence of the derived ambient electric field on the aspect ratio for thundercloud pressure

The ambient field E_{bg} required for corona onset can be derived from the onset field E_0 at the hydrometeor tip. This is done by simulating the hydrometeor as a conductor without surface charge in an ambient electric field in COMSOL, and increasing this field until the determined E_0 is obtained at the tip. The relative gas density of $\delta = 0.5$ and the most representative size of $C = 0.01\,\text{cm}^3$ (as hydrometeors are generally found in the millimeter range (Weinheimer et al., 1991; Gardiner et al., 1985)) are chosen. The results are presented in Figure 8. It is seen that the required background field E_{bg} is below the breakdown field E_k, between $0.07\,E_k$ and $0.8\,E_k$, and is lowest for the sharpest hydrometeor tips.

4 Summary, Conclusions and Outlook

The corona inception criterion set up by Naidis (2005) is applied through numerical simulations to spheroidal electrodes of various dimensions at different pressures. By doing so, the theoretical onset of a positive corona from an ellipsoidal hydrometeor is studied. It is found that the onset electric field at the hydrometeor tip decreases with hydrometeor volume and tip bluntness, as the hydrometeor surface near the photon absorption region increases with these factors. Moreover, the onset field increases with pressure due to the quenching of excited nitrogen molecules. For a hydrometeor of $0.042\,\text{cm}^3$ volume ($C = ab^2 = 0.01\,\text{cm}^3$) and thundercloud pressure ($\delta = 0.5$), the onset field at the tip varies approximately from $2.4E_k$ (limiting case sphere) to $70E_k$ (sharpest case considered), where E_k is the breakdown field. However, the onset field at the tip is not
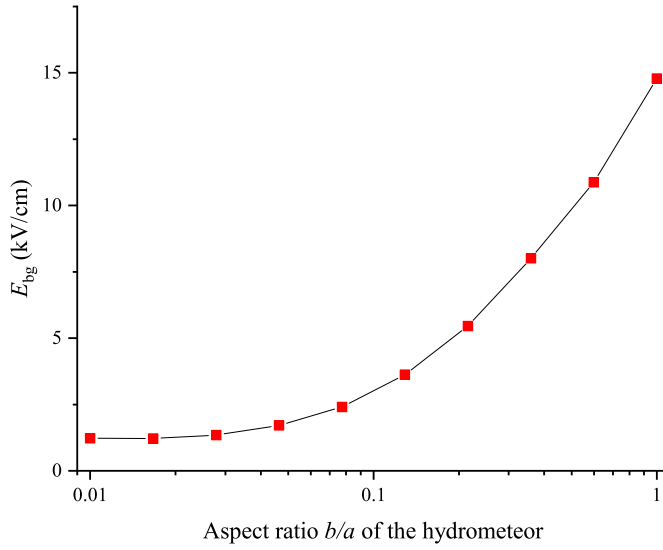
Figure 7. The a) onset field, b) onset charge, c) ionization integral for positive coronae at the tip of the ellipsoidal hydrometeor for $\delta = 10, 1, 0.5$, and 0.1 for varying aspect ratio b/a at a fixed volume parameter $C = 0.01\,\mathrm{cm}^3$. Results are compared in the spherical limit $(b = a)$ with Liu et al. (2012).

478   deemed representative for the likeliness of corona onset as it does not provide informa-
479   tion on the entire surface. These values were also obtained without the inclusion of an
480   ambient electric field. Instead, the onset potential difference, V_0, can provide a more re-
481   alistic picture for corona onset, since it can be compared with experimental results. As
482   we can observe, sharper hydrometeors need a lower voltage to initiate a discharge.

483   Another way to better predict the feasibility of corona onset in thundercloud elec-
484   tric fields is by the derivation of the required ambient electric field E_{bg} from the com-
485   puted onset field E_0. This yields values between $0.07\,E_k$ and $0.8\,E_k$ for semi-axes aspect
486   ratios between 0.01 and 1. Hence, the found ambient electric field is well below the break-
487   down field. It should be noted that this derived ambient field is neither an upper limit
488   nor lower limit on the field required for onset. While the model gives a minimum con-
489   dition for corona onset, the found E_0 would be lower if an ambient electric field was in-
490   cluded in the model in the first place. Thus, the used assumptions and simplifications
491   should be kept in mind when interpreting these results. However, the ambient field be-
492   ing significantly lower than the breakdown field for representative shapes is very promis-
493   ing.

Figure 8. The required background electric field, E_{bg}, to have an enhanced electric field of E_0 at the tip of the hydrometeor ($C = 0.01 \, \mathrm{cm}^3$). The values are calculated at $\delta = 0.5$, where $E_k = 17.9 \, \mathrm{kV/cm}$.

Whereas the onset field only provides information on the hydrometeor tip and the onset voltage only on the major axis, the onset charge is the total charge on the hydrometeor surface. This onset charge reveals, depending on hydrometeor volume, an optimal semi-axes aspect ratio of the ellipsoidal hydrometeor for which the least amount of charge is required for positive corona onset. The minimum in the onset charge curve is caused by the interplay between required onset field and geometry; a sharper hydrometeor has a larger onset field at the tip and thus requires more charge at the tip, but a larger part of its total charge is located at the tip. As this optimum was not found for the onset field or onset voltage, this suggests that considering only the major axis, which is often done in models for simplification, may not be sufficient when investigating corona onset conditions. Interestingly, in their study on lightning inception from hydrometeors, simulated as dielectrics in an ambient electric field, Dubinova et al. (2015) obtain a length-dependent optimum aspect ratio of the hydrometeor that requires the lowest ambient field for discharge inception. In addition, the obtained results can be compared to measured precipitation charges. Generally the hydrometeor charge is measured below 400 pC (Marshall & Winn, 1982). For the volume closest to the measured precipitation, $C = 0.01 \, \mathrm{cm}^3$, and a relative gas density of $\delta = 0.5$ the onset charge is found to be between and 1500 pC and 3100 pC. However, these charges were measured for estimated hydrometeor diameters between 1 and 3 mm, whereas in the spherical limit the simulated hydrometeors have diameters between 4 mm and 9 mm. In their simulations on spherical hydrometeors using the same corona inception criterion as this paper, Liu et al. have shown that the onset charge varies over several orders of magnitude in the estimated size range of hydrometers. For spherical hydrometeors of 9 mm diameter, the simulated onset charge was near ten times larger than for a 3 mm diameter. With this size correction (roughly a factor 10) onset charge values are close to the hydrometeors charges obtained from in situ measurements. Moreover, the considered configuration is an isolated hydrometeor with zero ambient field. Interaction between hydrometeors (see for example (Rutjes et al., 2019)) and a non-zero ambient field would lower the amount of charge required for

corona inception, which explains why the found onset charge is higher than expected from in-situ measurements.

Besides the onset charge, the ionization integral K also displays different behaviour in different b/a regions. For hydrometeors with very blunt tips, close to a spherical shape, a larger hydrometeor has a larger K value for onset, as photons are absorbed closer to the hydrometeor with respect to its size. However, for hydrometeors with sufficiently sharp tips, the absolute size of the photon absorption region seems to be more important than its relative size, such that a smaller hydrometeor has a larger value of the ionization integral. For any ellipsoidal shape, the value of the ionization integral is larger at higher pressures, because of the quenching of excited nitrogen molecules, which leads to lessened photon emission and therefore a need for stronger avalanches for corona onset.

To investigate the validity of the results, the approximations and assumptions of the model should be evaluated. Firstly, the distance r_{max} from the tip to the edge of the photon absorption region should be smaller than the hydrometeor length. Using the expression derived in the supporting information, it is found that for all data points the maximum ratio of this distance to length is $r_{max}/L = 0.2$, meaning this condition for the model to hold is satisfied. Furthermore, the presence of space charges is ignored in the model, leading to an overestimation of the electric field magnitude. When the ionization integral K, or equivalently number of electrons in the avalanche, is large enough, the perturbation of the electric field by the space charge becomes comparable to the magnitude of the electric field itself, such that space charge cannot be neglected. This is accompanied by the transformation of the avalanche into a streamer. In literature, it is often taken that K should be below 14-22 (Naidis, 2005; Raizer, 1991c) for the perturbation of the electric field by space charge to be neglected. In the results, the value of K is below this threshold for sufficiently blunt hydrometeors. Near $b/a = 0.555$ in Figure 6, which is also the cross-over point of the three curves, this value rises above 14. Hence, for sharper ellipsoids possibly more physics should be added to the model to obtain more accurate results.

In the model of the current work, it is assumed that there are sufficient free electrons present for the primary electron avalanche. To be able to draw conclusions on whether corona onset is possible in thunderclouds, it should be considered how these free electrons are supplied, and if this supply is large enough. The source of free electrons for lightning initiation is a widely researched subject, see for example (Dubinova, 2016; Rutjes et al., 2019). At least one primary electron is required for discharge initiation, but more electrons lower the inception threshold. When more electrons are available, the requirements on the other factors, such as the aspect ratio and volume of the hydrometeor or amplitude of the ambient field, will be softened.

From the above considerations, it can be concluded that lightning initiation from a spheroidal hydrometeor is feasible. While the onset field at the tip of the charged hydrometeor without ambient field was not found to be below the breakdown field in the considered configuration, the derived onset ambient electric field for the uncharged hydrometeor is lower than this threshold. Further enhancement could be provided by the interaction between hydrometeors. For representative dimensions and pressures, the amount of charge required for corona onset provided by the model is comparable to measured hydrometeor charges. Whether sharper hydrometeors promote lightning onset is a delicate discussion, which depends on which parameters are considered. From our results, it appears that only considering the major axis is not sufficient to reach conclusions on this matter. To further investigate the corona onset from hydrometeors using this model, more physics could be included. Most importantly, the thundercloud ambient electric field could be added to the model. Furthermore, the method can be applied to a hydrometeor cluster. The role of humidity, which was studied by Liu et al. (2012) for spherical hydrometeors, and the low-temperature environment can also be investigated. Finally, the model could be adjusted to account for space charge effects.

Appendix A Derivation of the distance ρ_0

To find the distance ρ_0 from the major axis to the surface of the ellipsoid along the surface electric field direction, the equation defining the ellipsoid (with the origin at the tip of the ellipsoid)

$$\frac{x^2}{b^2} + \frac{y^2}{b^2} + \frac{(z+a)^2}{a^2} = 1 \tag{A1}$$

is reformulated in spherical coordinates, which yields

$$\frac{r^2 \sin^2(\theta)}{b^2} + \frac{(a + r\cos(\theta))^2}{a^2} = 1. \tag{A2}$$

Solving equation (A2) for r gives two solutions, valid separately for $\theta \leq \pi/2$ and $\theta > \pi/2$, namely

$$r = \begin{cases} 0 & \theta \leq \pi/2 \\ \frac{2ab^2 \cos(\theta)}{(a^2 - b^2)\cos^2(\theta) - a^2} & \theta > \pi/2, \end{cases} \tag{A3}$$

as the range $\theta \leq \pi/2$ is the ionization region, which only encompasses the tip, $r = 0$, of the ellipsoidal surface (see also Figure 2). Substituting these solutions into the expression for ρ_{ab} (equation (4) and supporting information), thus constraining ρ_{ab} to the surface of the ellipsoid, gives

$$\rho_0 = \begin{cases} \dfrac{\left(a - \sqrt{a^2 - b^2}\right)\sqrt{2a\left(\sqrt{a^2 - b^2} + a\right) - b^2}}{a} & \theta \leq \pi/2 \\[3ex] \dfrac{4\left(2a\left(\sqrt{a^2-b^2}-a\right)+b^2+p_2\right)\sqrt{\dfrac{\left(\frac{4ab^2\left(2\sqrt{a^2-b^2}\right)\cos^2(\theta)}{(a^2-b^2)\cos^2(\theta)-a^2}+2a\left(\sqrt{a^2-b^2}+a\right)-b^2-p_2\right)\left(\frac{4ab^2\sqrt{a^2-b^2}\cos^2(\theta)}{(a^2-b^2)\cos^2(\theta)-a^2}+b^2+\frac{p_1}{8}-p_2\right)}{p_1}}}{2a\left(\sqrt{a^2-b^2}-a\right)+b^2-\frac{p_1}{8}+p_2} & \theta > \pi/2, \end{cases} \tag{A4}$$

with

$$p_1 = 8\rho_1 \rho_2 \left(r = \frac{2ab^2 \cos(\theta)}{(a^2 - b^2)\cos^2(\theta) - a^2} \right)$$

and

$$p_2 = -\rho_1{}^2 \left(r = \frac{2ab^2 \cos(\theta)}{(a^2 - b^2)\cos^2(\theta) - a^2} \right) - 2a\left(\sqrt{a^2 - b^2} - a \right) - b^2$$

Acknowledgments

The data that support the findings of this study are available from the corresponding author, S. A. Peeters, upon reasonable request. The MATLAB scripts used to generate the data for this paper and the full derivations of the indicated expressions are included in the supporting information.

References

Babich, L., Bochkov, E., & Neubert, T. (2017). The role of charged ice hydrometeors in lightning initiation. *Journal of Atmospheric and Solar-Terrestrial Physics*, *154*, 43 - 46. Retrieved from `http://www.sciencedirect.com/science/article/pii/S1364682616304564` doi: https://doi.org/10.1016/j.jastp.2016.12.010

Babich, L. P., Bochkov, E. I., Kutsyk, I. M., Neubert, T., & Chanrion, O. (2016). Positive streamer initiation from raindrops in thundercloud fields. *Journal of Geophysical Research: Atmospheres*, *121*(11), 6393-6403. Retrieved from `https://agupubs.onlinelibrary.wiley.com/doi/abs/10.1002/2016JD024901` doi: https://doi.org/10.1002/2016JD024901

Bandel, H. W. (1951, Oct). Point-to-plane corona in dry air. *Phys. Rev.*, *84*, 92–99. Retrieved from `https://link.aps.org/doi/10.1103/PhysRev.84.92` doi: 10.1103/PhysRev.84.92

Bolsig+ solver ver. windows 12/2019. (n.d.). Retrieved from `http://www.bolsig.laplace.univ-tlse.fr/`

Coquillat, S., Chauzy, S., & Médale, J.-C. (1995). Microdischarges between ice particles. *Journal of Geophysical Research: Atmospheres*, *100*(D7), 14327-14334. Retrieved from `https://agupubs.onlinelibrary.wiley.com/doi/abs/10.1029/95JD00986` doi: https://doi.org/10.1029/95JD00986

Crabb, J. A., & Latham, J. (1974). Corona from colliding drops as a possible mechanism for the triggering of lightning. *Quarterly Journal of the Royal Meteorological Society*, *100*(424), 191-202. Retrieved from `https://rmets.onlinelibrary.wiley.com/doi/abs/10.1002/qj.49710042406` doi: https://doi.org/10.1002/qj.49710042406

Curtright, T. L., Cao, Z., Huang, S., Sarmiento, J. S., Subedi, S., Tarrence, D. A., & Thapaliya, T. R. (2020, apr). Charge densities for conducting ellipsoids. *European Journal of Physics*, *41*(3), 035204. Retrieved from `https://doi.org/10.1088%2F1361-6404%2Fab806a` doi: 10.1088/1361-6404/ab806a

D'Alessandro, F., & Berger, G. (1999, oct). Laboratory studies of corona emissions from air terminals. *Journal of Physics D: Applied Physics*, *32*(21), 2785–2790. Retrieved from `https://doi.org/10.1088%2F0022-3727%2F32%2F21%2F311` doi: 10.1088/0022-3727/32/21/311

Dubinova, A. (2016). *Modeling of streamer discharges near dielectrics* (Unpublished doctoral dissertation). Department of Applied Physics. (Proefschrift)

Dubinova, A., Rutjes, C., Ebert, U., Buitink, S., Scholten, O., & Trinh, G. T. N. (2015, Jun). Prediction of lightning inception by large ice particles and extensive air showers. *Phys. Rev. Lett.*, *115*, 015002. Retrieved from `https://link.aps.org/doi/10.1103/PhysRevLett.115.015002` doi: 10.1103/PhysRevLett.115.015002

Dwyer, J. R., & Uman, M. A. (2014). The physics of lightning. *Physics Reports*, *534*(4), 147–241.

Gardiner, B., Lamb, D., Pitter, R. L., Hallett, J., & Saunders, C. P. R. (1985). Measurements of initial potential gradient and particle charges in a montana summer thunderstorm. *Journal of Geophysical Research: Atmospheres*, *90*(D4), 6079-6086. Retrieved from `https://agupubs.onlinelibrary.wiley.com/doi/abs/10.1029/JD090iD04p06079` doi: https://doi.org/10.1029/JD090iD04p06079

Griffiths, R. (1975). The initiation of corona discharges from charged ice particles in a strong electric field. *Journal of Electrostatics*, *1*(1), 3 - 13. Retrieved from `http://www.sciencedirect.com/science/article/pii/0304388675900030` doi: https://doi.org/10.1016/0304-3886(75)90003-0

Griffiths, R. F., & Latham, J. (1974). Electrical corona from ice hydrometeors. *Quarterly Journal of the Royal Meteorological Society*, *100*(424), 163-180. Retrieved from `https://rmets.onlinelibrary.wiley.com/doi/abs/10.1002/`

qj.49710042404 doi: https://doi.org/10.1002/qj.49710042404

Hagelaar, G. J. M., & Pitchford, L. C. (2005, October). Solving the Boltzmann equation to obtain electron transport coefficients and rate coefficients for fluid models. *Plasma Sources Sci. Technol.*, *14*(4), 722–733. doi: 10.1088/0963-0252/14/4/011

Itikawa, Y. (2005, December). Cross Sections for Electron Collisions with Nitrogen Molecules. *Journal of Physical and Chemical Reference Data*, *35*(1), 31–53. (Publisher: American Institute of Physics) doi: 10.1063/1.1937426

Itikawa, Y. (2008, December). Cross Sections for Electron Collisions with Oxygen Molecules. *Journal of Physical and Chemical Reference Data*, *38*(1), 1–20. (Publisher: American Institute of Physics) doi: 10.1063/1.3025886

Itikawa database, www.lxcat.net, retrieved on sep 15, 2020. (n.d.).

Kip, A. F. (1938, Jul). Positive-point-to-plane discharge in air at atmospheric pressure. *Phys. Rev.*, *54*, 139–146. Retrieved from https://link.aps.org/doi/10.1103/PhysRev.54.139 doi: 10.1103/PhysRev.54.139

Köhn, C., & Ebert, U. (2015). Calculation of beams of positrons, neutrons, and protons associated with terrestrial gamma ray flashes. *Journal of Geophysical Research: Atmospheres*, *120*(4), 1620-1635. Retrieved from https://agupubs.onlinelibrary.wiley.com/doi/abs/10.1002/2014JD022229 doi: https://doi.org/10.1002/2014JD022229

Liu, N., Dwyer, J. R., & Rassoul, H. K. (2012). Effects of pressure and humidity on positive corona inception from thundercloud hydrometeors. *Journal of Atmospheric and Solar-Terrestrial Physics*, *80*, 179 - 186. Retrieved from http://www.sciencedirect.com/science/article/pii/S1364682612000260 doi: https://doi.org/10.1016/j.jastp.2012.01.012

Loeb, L. B. (1966). The mechanisms of stepped and dart leaders in cloud-to-ground lightning strokes. *Journal of Geophysical Research (1896-1977)*, *71*(20), 4711-4721. Retrieved from https://agupubs.onlinelibrary.wiley.com/doi/abs/10.1029/JZ071i020p04711 doi: https://doi.org/10.1029/JZ071i020p04711

MacGorman, D., MacGorman, R., Rust, W., & Rust, W. (1998). *The electrical nature of storms.* Oxford University Press. Retrieved from https://books.google.nl/books?id=_NbHNj7KJecC

Marshall, T. C., McCarthy, M. P., & Rust, W. D. (1995). Electric field magnitudes and lightning initiation in thunderstorms. *Journal of Geophysical Research: Atmospheres*, *100*(D4), 7097-7103. Retrieved from https://agupubs.onlinelibrary.wiley.com/doi/abs/10.1029/95JD00020 doi: https://doi.org/10.1029/95JD00020

Marshall, T. C., & Winn, W. P. (1982). Measurements of charged precipitation in a new mexico thunderstorm: lower positive charge centers. *Journal of Geophysical Research: Oceans*, *87*(C9), 7141-7157. Retrieved from https://agupubs.onlinelibrary.wiley.com/doi/abs/10.1029/JC087iC09p07141 doi: https://doi.org/10.1029/JC087iC09p07141

Mazur, V. (2016). *Principles of lightning physics.* IOP Publishing. Retrieved from http://dx.doi.org/10.1088/978-0-7503-1152-6 doi: 10.1088/978-0-7503-1152-6

Naidis, G. V. (2005, jun). Conditions for inception of positive corona discharges in air. *Journal of Physics D: Applied Physics*, *38*(13), 2211–2214. Retrieved from https://doi.org/10.1088\%2F0022-3727\%2F38\%2F13\%2F020 doi: 10.1088/0022-3727/38/13/020

Nasser, E., & Heiszler, M. (1974, August). Mathematical-physical model of the streamer in nonuniform fields. *Journal of Applied Physics*, *45*(8), 3396-3401. doi: 10.1063/1.1663791

Petersen, D., Bailey, M., Beasley, W. H., & Hallett, J. (2008). A brief review of the problem of lightning initiation and a hypothesis of initial lightning leader formation. *Journal of Geophysical Research: Atmospheres*, *113*(D17).

Retrieved from `https://agupubs.onlinelibrary.wiley.com/doi/abs/` `10.1029/2007JD009036` doi: https://doi.org/10.1029/2007JD009036

Petersen, D., Bailey, M., Hallett, J., & Beasley, W. (2015). Laboratory investigation of corona initiation by ice crystals and its importance to lightning. *Quarterly Journal of the Royal Meteorological Society*, *141*(689), 1283-1293. Retrieved from `https://rmets.onlinelibrary.wiley.com/doi/abs/10.1002/qj.2436` doi: https://doi.org/10.1002/qj.2436

Petersen, D., Bailey, M., Hallett, J., & Beasley, W. H. (2006). Laboratory investigation of positive streamer discharges from simulated ice hydrometeors. *Quarterly Journal of the Royal Meteorological Society*, *132*(615), 263-273. Retrieved from `https://rmets.onlinelibrary.wiley.com/doi/abs/10.1256/qj.05.32` doi: https://doi.org/10.1256/qj.05.32

Phelps, C. (1974). Positive streamer system intensification and its possible role in lightning initiation. *Journal of Atmospheric and Terrestrial Physics*, *36*(1), 103 - 111. Retrieved from `http://www.sciencedirect.com/science/article/pii/0021916974900701` doi: https://doi.org/10.1016/0021-9169(74)90070-1

Phelps, C. T., & Griffiths, R. F. (1976). Dependence of positive corona streamer propagation on air pressure and water vapor content. *Journal of Applied Physics*, *47*(7), 2929-2934. Retrieved from `https://doi.org/10.1063/1.323084` doi: 10.1063/1.323084

Phelps database, www.lxcat.net, retrieved on sep 15, 2020. (n.d.).

Raizer, Y. P. (1991a). *Gas discharge physics. Fizika gazovogo razryada.* Berlin: Springer. Retrieved from `https://cds.cern.ch/record/264408` (Translated from Russian by Vitaly I Kisin)

Raizer, Y. P. (1991b). *Gas discharge physics. Fizika gazovogo razryada.* Berlin: Springer. Retrieved from `https://cds.cern.ch/record/264408` (Translated from Russian by Vitaly I Kisin)

Raizer, Y. P. (1991c). *Gas discharge physics. Fizika gazovogo razryada.* Berlin: Springer. Retrieved from `https://cds.cern.ch/record/264408` (Translated from Russian by Vitaly I Kisin)

Riousset, J. A., Nag, A., & Palotai, C. (2020). Scaling of conventional breakdown threshold: Impact for predictions of lightning and tles on earth, venus, and mars. *Icarus*, *338*, 113506. Retrieved from `http://www.sciencedirect.com/science/article/pii/S0019103519305688` doi: https://doi.org/10.1016/j.icarus.2019.113506

Rison, W., Krehbiel, P. R., Stock, M. G., Edens, H. E., Shao, X.-M., Thomas, R. J., . . . Zhang, Y. (2016). Observations of narrow bipolar events reveal how lightning is initiated in thunderstorms. *Nature communications*, *7*, 10721. Retrieved from `https://europepmc.org/articles/PMC4756383` doi: 10.1038/ncomms10721

Rutjes, C. (2018). *Modeling high energy atmospheric physics and lightning inception* (Unpublished doctoral dissertation). Department of Applied Physics. (Proefschrift)

Rutjes, C., Ebert, U., Buitink, S., Scholten, O., & Trinh, T. N. G. (2019). Generation of seed electrons by extensive air showers, and the lightning inception problem including narrow bipolar events. *Journal of Geophysical Research: Atmospheres*, *124*(13), 7255-7269. Retrieved from `https://agupubs.onlinelibrary.wiley.com/doi/abs/10.1029/2018JD029040` doi: 10.1029/2018JD029040

Schumann, W. (1923, June). Über das minimum der durchbruchfeldstärke bei kugelelektroden. *Archiv f. Elektrotechnik*, 593—608. Retrieved from `https://doi.org/10.1007/BF01656766`

Stolzenburg, M., & Marshall, T. C. (2009). Electric field and charge structure in lightning-producing clouds. In H. D. Betz, U. Schumann, & P. Laroche

(Eds.), *Lightning: Principles, instruments and applications: Review of modern lightning research* (pp. 57–82). Dordrecht: Springer Netherlands. Retrieved from `https://doi.org/10.1007/978-1-4020-9079-0_3` doi: 10.1007/978-1-4020-9079-0_3

Wantzel, L. (1843). Classification des nombres incommensurables d'origine algébrique. *Nouvelles annales de mathématiques : journal des candidats aux écoles polytechnique et normale*, *1e série, 2*, 117-127. Retrieved from `http://www.numdam.org/item/NAM_1843_1_2__117_1`

Waters, R. T., & Stark, W. B. (1975, mar). Characteristics of the stabilized glow discharge in air. *Journal of Physics D: Applied Physics*, *8*(4), 416–426. Retrieved from `https://doi.org/10.1088%2F0022-3727%2F8%2F4%2F014` doi: 10.1088/0022-3727/8/4/014

Weinheimer, A. J., Dye, J. E., Breed, D. W., Spowart, M. P., Parrish, J. L., Hoglin, T. L., & Marshall, T. C. (1991). Simultaneous measurements of the charge, size, and shape of hydrometeors in an electrified cloud. *Journal of Geophysical Research: Atmospheres*, *96*(D11), 20809-20829. Retrieved from `https://agupubs.onlinelibrary.wiley.com/doi/abs/10.1029/91JD02262` doi: https://doi.org/10.1029/91JD02262

Zhelezniak, M. B., Mnatsakanian, A. K., & Sizykh, S. V. (1982, November). Photoionization of nitrogen and oxygen mixtures by radiation from a gas discharge. *High Temperature Science*, *20*(3), 357-362.